Assessment of classical, advanced, and layer-wise theories for the vibration of rotating composite anisotropic blades

Assessment of classical, advanced, and layer-wise theories for the vibration of rotating composite anisotropic blades

M. Filippi*, D. Giusa, A. Pagani, E. Zappino, E. Carrera

Mul^2 group, Department of Mechanical and Aerospace Engineering
Politecnico di Torino, Italy

Abstract

The present paper aims at studying composite cambered structures, tracking the seminar work "Rotating Blade Vibration Analysis Using Shells" presented by Leissa in Journal of Engineering for Power, in 1982, devoted to homogeneous metallic blades. A refined unidimensional (1D) formulation is here implemented to overcome the limitations of classical beam theories. With an appropriate choice of cross-sectional expansions, it is possible to make the 1D model suitable for analyzing shallow blades. This approach enables one to generate both layerwise (LW) and equivalent single layer (ESL) descriptions of the problem unknowns. Furthermore, it is possible to implement classic theories as special cases. Natural frequencies are determined for isotropic and composite blades, showing the effects of changing the fiber lamination angle of symmetric and unsymmetric configurations. Besides, this study investigates the effects of thickness and rotational speed over the structure. Significant differences between classic and high-order theories are found, concerning the accuracy and the computational costs. The causes of these differences are discussed, and the results can be used as a benchmark for future studies.

Keywords: Rotordynamics, Finite element, Beam, Carrera Unified Formulation (CUF), Laminated Blades

1. Introduction

Vibration analysis of rotating blades is a central problem in the rotordynamics and aerospace field, and they have been extensively carried out in recent decades. The commercial interest of the rotating blade is well-known, and they find many applications in several components such as compressors, turbines, propellers, and helicopter rotors. Several investigations have been understanding to reduce noise, increase efficiency, and avoid catastrophic failure. To achieve these goals knowing the dynamic

*Corresponding author. E-mail matteo.filippi@polito.it

characteristics of these structures is essential, and a correct approach is required to describe the modal aberrations correctly. A considerable number of references can be found in the literature; many of them have been focused on beam formulations. Rao [1] defined the governing equations in terms of a single coordinate corresponding at the main axis of the structure. Putter and Manor [2] established a finite element method (FEM) to study the natural frequencies of radial beams mounted on a rotating disk. This FEM model incorporated shear effects, rotary inertia, and varying centrifugal forces. Chandra and Chopra [3] carried out an analysis of composite box beams utilizing a Newtonian approach along with the Galerkin method. Hodges et al. [4, 5] proposed a variational asymptotic beam sectional analysis (VABS), in which the blade analysis is divided into a linear two-dimensional (2D) problem over the cross-section and a nonlinear analysis along the coordinate of the beam axis. Beam formulations can be highly inaccurate in the case of thin-walled structures, small aspect ratio, and large chordwise chamber. Many authors overcame these limitations by employing shell formulation [6–8]. Yu et al. [9], extended VABS to 2D problems, in which the analysis were performed through an equivalent single layer (ESL) approach. The multi flexible-body code DYMORE is mentioned in the literature [10], and it finds numerous applications in the rotorcraft field [11, 12]. Leissa and Ewing [13] presented an accurate survey of the one- and two- dimensional theories and made quantitative comparisons of frequencies obtained for turbomachinery blades. Moreover, Leissa, with his coworkers, conducted several studies by developing both beam and shell formulations [14, 15]. For composite structures a shallow-shell theory was presented by Qatu and Leissa in Ref. [16], in which the first known natural frequencies and mode shapes of laminated pre-twisted cantilever plates were calculated. In recent years Sun et al. developed a two-dimensional model for multilayer rotating blades using a quadratic layerwise theory. A comprehensive description of this model can be found in Ref. [17], in which results of numerical simulations are compared to the full three-dimensional model showing an excellent

agreement.

Many papers have been recently published to extend Carrera Unified Formulation (CUF) to the rotordynamics analysis. Carrera et al. [18] compared, with published solutions, the natural frequencies of rotating beams with compact cross-sections and open profiles made of either isotropic or orthotropic materials. Carrera and Filippi [19, 20] investigated the dynamic behavior of metallic and composite rotors by utilizing both TE and LE beam elements. The formulation encompassed all contributions due to the rotation, namely the Coriolis term, the spin-softening matrix, and the stress-stiffening matrix. The several comparisons presented in those papers demonstrated that beam CUF models were a viable alternative to FE solutions of higher dimensionality. Moreover, an accurate nonlinear dynamics analysis was presented in Ref. [21], showed relevant discrepancies when structures with deep curvatures were considered. Despite the considerable amount of papers devoted to the dynamics of rotating blades, it seems that there is a gap in the vibration analysis of evaluating the accuracy of theories for rotating composite blades incompatible with the growing popularity of composite structures. The purpose of this paper is to providing reference results for composite rotating blades that can be used as a benchmark for future studies. The present research is inspired by Leissa's paper [15] in which the effects of the thickness, of the angular velocity, and the kinematic theories on the natural frequencies of the blade were evaluated. This study is done in the framework of CUF approach that permits to adopt two different models to the focus on the composite blades, namely the equivalent single layer (ESL) theory and the layer-wise (LW) models.

2. Description of the employed theories

CUF for one-dimensional elements (1D) [22] expresses the displacement field $\mathbf{u}^T = [u_x\, u_y\, u_z]$ as an arbitrary expansions of cross-sectional functions $F_\tau(x, z)$ and the

generalized displacements $\mathbf{u}_\tau(y)$, along the beam axis y.

$$\mathbf{u} = F_\tau(x,z)\mathbf{u}_\tau(y) \quad \tau = 1,2,\ldots,M \tag{1}$$

where M is the number of terms of the expansions. If the finite element method is adopted, the generalized displacements are approximated using the shape functions, $N_i(y)$, and the vector of nodal displacement $\mathbf{u}_{i\tau}$. Therefore the displacement field is being approximated as:

$$\mathbf{u} = N_i(y)F_\tau(x,z)\mathbf{u}_{i\tau} \quad \tau = 1,...,M \quad i = 1,...,N_{nodes} \tag{2}$$

where the number of beam element nodes are denoted by N_{nodes}, τ is related to the expansion used for defining the cross-sectional kinematics and its maximum value, M, is an input parameter of the analysis. Moreover the parameter M is the number of expansions terms used to describe the cross-section behavior. N defines the polynomial order for the Taylor-type models, named TEN. Theories for multilayered structures can be developed by making an appropriate choice of the variable description, in this sense it is possible to distinguish two categories: equivalent single layer (ESL) models or layer-wise (LW) models. The ESLs theories consider a number of unknown variables that are independent of the number of constitutive layers. These theories lead to a homogeneous approach, indeed the kinematics of the structure is insensitive to individual layers, unless Zig-Zag models are used (more detail in Ref. [23]).

ESL models are based on theories that are originally developed for single layer structures made of traditional isotropic materials. Their application on multilayered structured lead to specific theories for composite plate and shells [24, 25]. The ESL theories include the classical laminated theory, the first-order deformation theories, and higher-order deformation theories. These theories will be briefly described below and applied to the structure. More details for each theories can be found in Ref.

[26].

2.1. Classical ESL theory

2.1.1. The Euler-Bernoulli Beam Theory (EBBT)

The EBBT is derived from three a-priori assumptions. The first assumes that the cross-section is rigid on its plane. For the second hypothesis, the cross-section remains perpendicular to the neutral surface during deformation. And for the last assumption, the cross-section rotates around a neutral surface remaining plane. Based on the first hypothesis, in-plane displacement are not considered for EBBT, and consequently, the in-plane displacements $u_x(y)$ and $u_z(y)$ depend on the axial coordinate y. For the second hypothesis, the out-of-plane or axial displacement u_y is linear versus the in-plane coordinates: For the third hypothesis and based on the shear strains definition, shear deformations γ_{yz} and γ_{yx} are disregarded:

$$\gamma_{yz} = \gamma_{yx} = 0$$

The rotation angles can obtained as functions of the derivatives of the in-plane displacements. The displacement field, $\mathbf{u}^T = [u_x\, u_y\, u_z]$, of EBBT is then:

$$\begin{aligned} u_x &= u_{x_1} \\ u_y &= u_{y_1} - u_{x_1,y}x - u_{z_1,y}z \\ u_z &= u_{z_1} \end{aligned} \tag{3}$$

where the comma denotes a spatial derivative and the subscript 1 is referred to the displacement value with correspondence to the beam axis ($x = z = 0$)

2.1.2. The Timoshenko Beam Theory (TBT)

Timoshenko beam theory, or First order Shear Deformation Theory (FSDT), is an extension of Euler-Bernoulli beam model. The third kinematic assumption of the EBBT is removed for FSDT. The cross-section remains rigid on its plane, and it can

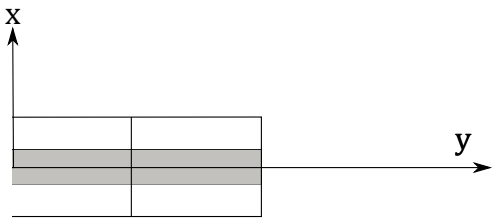

(a) *Undeformed configuration*

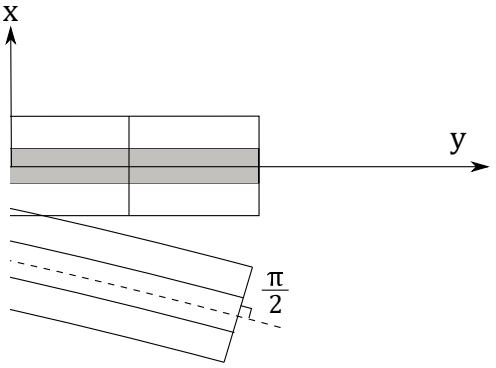

(b) *Euler-Bernoulli Beam Theory - EBBT*

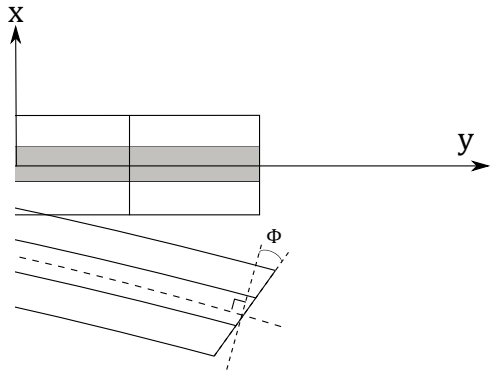

(c) *First order Shear Deformation Theory - FSDT*

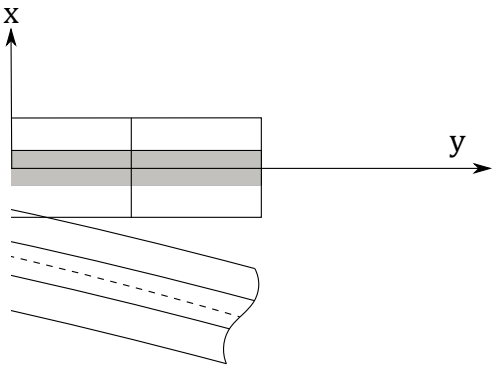

(d) *ESL High order*

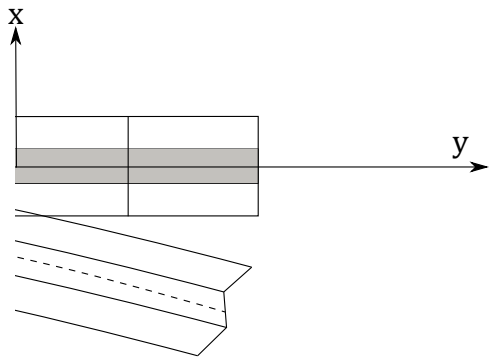

(e) *LW linear*

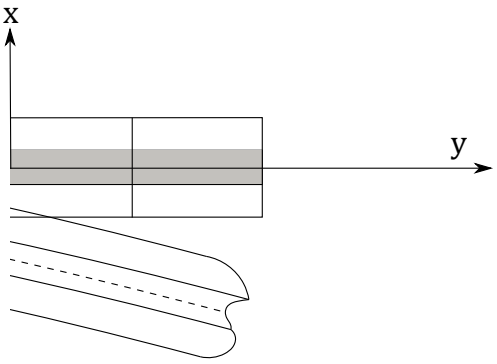

(f) *LW high order*

Figure 1: Theories assumptions in one-dimensional cases

rotate around a neutral surface while it remains plane. However, it is not constrained to be perpendicular to it (see Fig. 1(c)). Shear deformations γ_{xy} and γ_{yz} are now accounted for. The displacement field of the FSDT can be written as:

$$\begin{aligned} u_x &= u_{x_1} \\ u_y &= u_{y_1} + \phi_z x + \phi_x z \\ u_z &= u_{z_1} \end{aligned} \tag{4}$$

where ϕ_z and ϕ_x are the rotation angles along the z- and the x-axis, respectively.

2.2. Refined theories or higher order theories (HOT)

2.2.1. Linear type expansion theory (TE1)

The complete linear expansion model involves a first-order (TE1) Taylor-like polynomial to describe the cross-section displacement field,

$$\begin{aligned} u_x &= u_{x_1} + x u_{x_2} + z u_{x_3} \\ u_y &= u_{y_1} + x u_{y_2} + z u_{y_3} \\ u_z &= u_{z_1} + x u_{z_2} + z u_{z_3} \end{aligned} \tag{5}$$

where subscripts 2 and 3 are referred to the in-plane stretching terms. The present model introduces nine displacement variables: three constant ($u_{x_1}, u_{y_1}, u_{z_1}$) and six linear ($u_{x_2}, \ldots, u_{z_3}$). The ϵ_{xx}, ϵ_{zz} deformations and γ_{xz} rotation have a constant distribution above the cross-section, instead ϵ_{yy}, γ_{xy} and γ_{yz} assume a linear behavior. The adoption of the $N = 1$ model is necessary to introduce a linear distribution of the in-plane stretching, which cannot be detected by classical theories like EBBT and FSDT.

2.2.2. Higher-order type expansion theories (TE2,TE3,...,TEN)

More refined models are needed to describe mechanical response of structures that present complex boundary (e.g. torsion) or geometrical (e.g. thin walls) conditions. These models are needed to predict a number of non classical effects such as warping,

in-plane distortion and shear effects, a complete review of the major theories is provided by Carrera et al. in Ref. [27]. One possible choice deals with adoption of Taylor-like polynomials consisting of the 2D base $x^i\ z^j$, where i and j are positive integers. An example is given for a second order model (see Fig. 1(d)) that exploits a parabolic expansion of the Taylor-like polynomials,

$$\begin{aligned} u_x &= u_{x_1} + xu_{x_2} + zu_{x_3} + x^2u_{x_4} + xzu_{x_5} + z^2u_{x_6} \\ u_y &= u_{y_1} + xu_{y_2} + zu_{y_3} + x^2u_{y_4} + xzu_{y_5} + z^2u_{y_6} \\ u_z &= u_{z_1} + xu_{z_2} + zu_{z_3} + x^2u_{z_4} + xzu_{z_5} + z^2u_{z_6} \end{aligned} \tag{6}$$

The 1D model given by Eq. 6 has 18 displacement variables: three constant $(u_{x_1}, u_{y_1}, u_{z_1})$, six linear $(u_{x_2}, \ldots, u_{z_3})$ and nine parabolic $(u_{x_4}, \ldots, u_{z_6})$. The present beam formulation is able to implement any-order theory by choosing the expansion order, N.

2.3. Layer-wise theories

A layer-wise approach can be used if a detailed description of layers is required. An overview of layer-wise theories for composite laminates and structures was provided by Carrera [28]. The LW theories treat independent displacement fields in every single layer and then impose compatibility conditions at the interfaces between laminae. A linear and an high-order layer-wise z-expansion example are shown in Fig. 1(e) and 1(f), respectively. The unknown variables are only pure displacement if Lagrange polynomials are adopted as expansion functions (F_τ). Several types of cross-sectional polynomials sets can be adopted, some examples are shown in Fig. 2. The displacement field is:

$$\begin{aligned} u_x^k &= u_{x_1}^k F_1^k(x,z) + \cdots + u_{x_N}^k F_N^k(x,z) \\ u_y^k &= u_{y_1}^k F_1^k(x,z) + \cdots + u_{y_N}^k F_N^k(x,z) \\ u_z^k &= u_{z_1}^k F_1^k(x,z) + \cdots + u_{z_N}^k F_N^k(x,z) \end{aligned} \tag{7}$$

$k = 1, \ldots, N_{layers}$ denotes each layers. $F_1(x,z), \ldots, F_N(x,z)$ are the $1^{st}, \ldots, N^{th}$

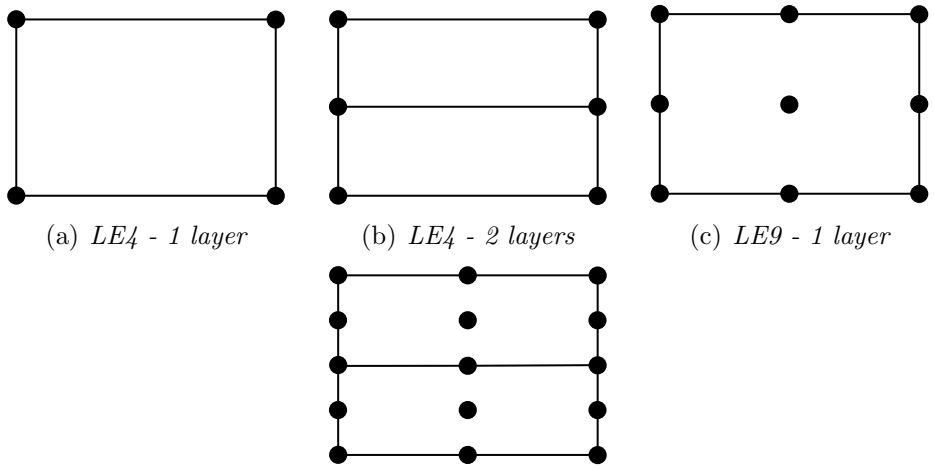

(a) *LE4 - 1 layer* (b) *LE4 - 2 layers* (c) *LE9 - 1 layer*

(d) *LE9 - 2 layers*

Figure 2: Cross-section L-elements for different numbers of layers. (a,b) Four-point element, LE4; (c,d) nine-point element, LE9.

order Lagrange polynomials. The Lagrange polynomials are usually given in terms of normalized - or natural - coordinates. This choice is not compulsory since LE polynomials can also be implemented in terms of actual coordinates. However, the normalized formulation was preferred since it offers many advantages. The simplest quadrilateral Lagrange polynomials (LE4) are:

$$F_\tau = \frac{1}{4}(1 + rr_\tau)(1 + ss_\tau) \qquad \tau = 1, 2, 3, 4 \tag{8}$$

where r and s are the normalized coordinates and r_τ and s_τ are the coordinates of the four points in a natural coordinate frame. In the case of an LE9 element, the interpolation functions are given by:

$$F_\tau = \frac{1}{4}(r^2 + rr_\tau)(s^2 + ss_\tau) \qquad \tau = 1, 3, 5, 7 \tag{9}$$

$$F_\tau = \frac{1}{2}s_\tau^2(s^2 + ss_\tau)(1 - r^2) + \frac{1}{2}r_\tau^2(r^2 + rr_\tau)(1 - s^2) \qquad \tau = 2, 4, 6, 8 \tag{10}$$

$$F_\tau = (1 - r^2)(1 - s^2) \qquad \tau = 9 \tag{11}$$

These models include constrain conditions in order to enforce the compatibility conditions at each layer interface. More details about LE models can be found in the paper by Carrera and Petrolo [29].

2.4. Rotordynamics equations

For the rotordynamic analysis of the blade, it is necessary to derive the equation of motion in a compatible form with the condensed formulation of the CUF. The equations of motion are derived through Hamilton's principle, which in the usual form reads:

$$\delta \int_{t_0}^{t_1} (T - U)\, dt = 0 \tag{12}$$

where T and U are the kinetic and the potential energies in the rotating reference frame and δ represents the virtual variation of the functional. The equation of motion is written in a form compatible with CUF:

$$\mathbf{M}\ddot{\mathbf{q}} + \mathbf{G}_\Omega \dot{\mathbf{q}} + (\mathbf{K} - \mathbf{K}_\Omega + \mathbf{K}_{\sigma_0})\mathbf{q} = 0 \tag{13}$$

The homogeneous equation is solved for the computation of natural frequencies, for more details see Ref. [30]. The arrays at Eq. 13 assume the following denomination:

- the mass matrix $\mathbf{M^{ij\tau s}}$
- the stiffness matrix $\mathbf{K^{ij\tau s}}$
- the Coriolis matrix $\mathbf{G^{ij\tau s}}$
- the centrifugal softening matrix $\mathbf{K_\Omega^{ij\tau s}}$
- the centrifugal stiffening matrix $\mathbf{K_{\sigma_0}^{ij\tau s}}$
- the load vector $\mathbf{F_\Omega^{ij\tau s}}$

Explicit form of these arrays can be found in previous authors' works [20, 31].

3. Numerical results

3.1. Geometry and material of the blade

To validate the methodology several benchmark problems available in the literature have been considered to examine the effect of the theory approximation order and the material anisotropy (material properties are shown in Table 1). Then, the effects of thickness and stacking sequences are investigated. The geometrical features of the blade are shown in Fig. 3, where $L = b = 30.5$ cm, $t = L/100$ and $R_x = 2b$. In the following analysis the hub-radius is considered equal to $r_h = 0.0$ m.

3.2. Finite elements adopted for the considered blade

Layerwise models are obtained by using a combination of 48 cubic LE9 polynomials over the blade cross-section as shown in Fig. 4. These elements are opportunely distributed so that the theory kinematics is independent for each layer, for both the two- and three-layer configurations. Along the y-axis have been used 8 beam elements with 4 nodes (B4). A detailed analysis of the effects of the number and the type of finite elements along the beam axis can be found in [26].

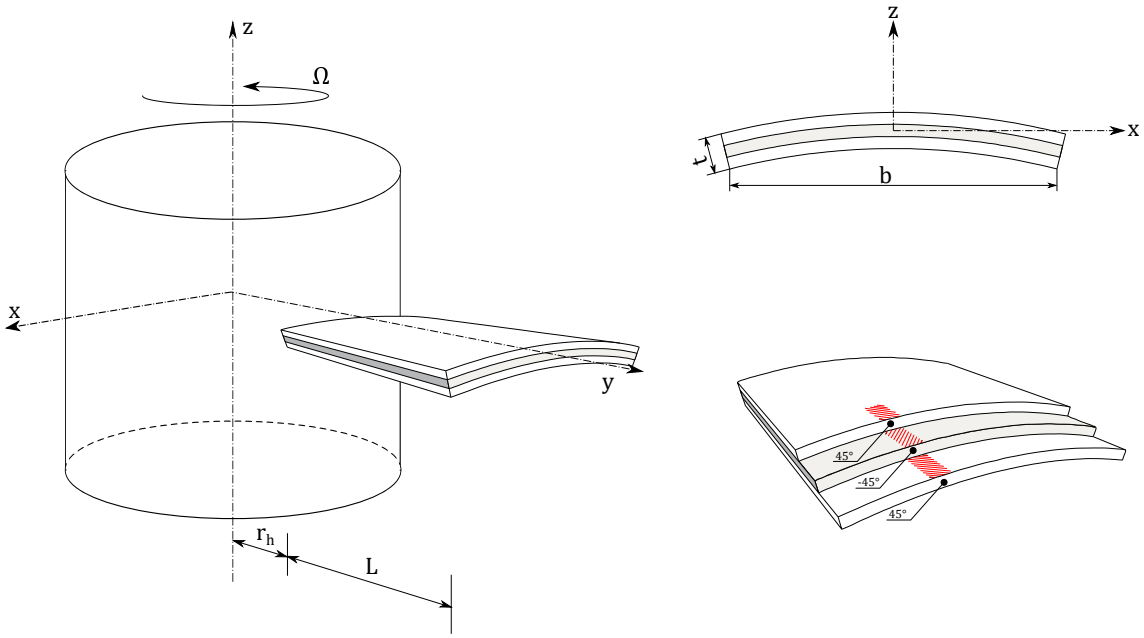

Figure 3: Sketch of a blade with an example of fibers lamination angles

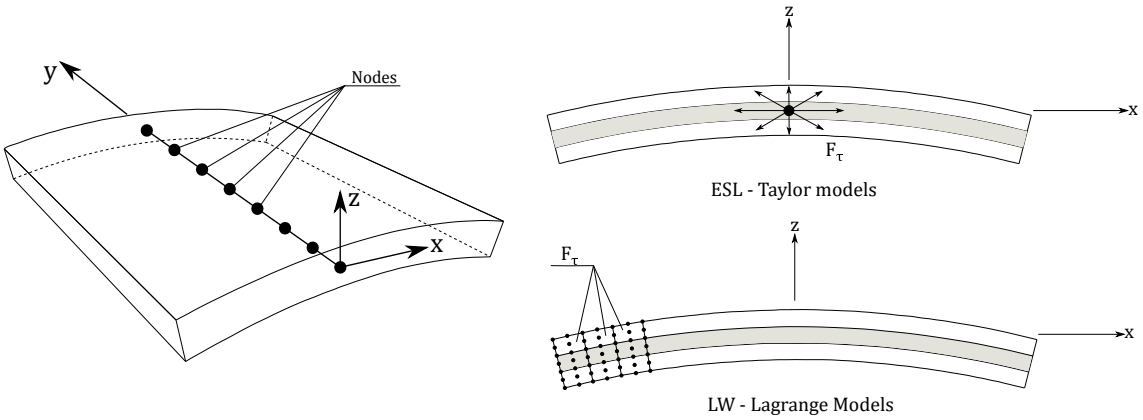

Figure 4: FEM nodes mesh along the y-axis and cross-sections discretization for ESL and LW models

Isotropic			**Graphite/epoxy**					
E	ν	ρ	$\mathbf{E_1}$	$\mathbf{E_3}$	$\mathbf{G_{13}}$	$\nu_{\mathbf{13}}$	$\nu_{\mathbf{13}}$	ρ
GPa	-	Kg/m^3	GPa	GPa	GPa	-	-	Kg/m^3
200	0.3	7860	181	10.3	7.17	0.28	0.33	1600

Table 1: Material properties

3.3. Free vibration analysis

For validation purposes, natural frequencies of an isotropic rotating blade were first calculated and compared to both experimental and analytical predictions. Higher-than-second-order Taylor models and Lagrange model showed a good agreement with those obtained with shell and solid solutions [15, 32], and with a Nastran analysis [21]. The results are tabulated in Tab. 2. Low-orders models revealed a low accuracy both in computing the values of the frequencies and in identifying the shape modes.

For the orthotropic material, several stacking sequences have been analyzed. All plies were assumed to have the same thickness. Histograms in Fig. 5 show differences in terms of natural frequencies between the various models (more details in Tab. 3 and 4), considering the same mode shapes among the first six modes of the structure (an example is provided in Fig. 6 for $[45°/-45°/45°]$ stacking sequence). Comparing the results with the reference case LE9, only TE5 and TE6

models have provided similar frequencies and comparable mode shapes. Frequencies of TE4 models were slightly different, and in some cases, this theory cannot detect correctly the mode shapes. For TE3, a satisfactory level of accuracy was found only for the first frequency, which was always the first torsional one. The poor accuracy of models TE1 and TE2 was evident, even for low-frequency modes. Finally, EBBT and FSDT models can provide natural frequencies only for bending modes with acceptable accuracy.

Model	**Natural frequencies**						**DoFs**
EBBT	176.77 $_{1f}$	1,102.22 $_{2f}$	2,264.59 $_{1l}$	3,061.56 $_{3f}$	4,134.70	5,931.11 $_{4f}$	75
FSDT	176.38 $_{1f}$	1,085.85 $_{2f}$	1,782.37 $_{1l}$	2,959.05 $_{3f}$	4,134.70	4,785.38 $_{4f}$	125
TE1	204.49 $_{1f}$	1,253.49 $_{2f}$	1,928.68 $_{1l}$	2,564.23 $_{1t}$	3,395.13 $_{3f}$	4,187.46	225
TE2	166.02 $_{1f}$	431.76 $_{1t}$	640.77 $_{2f}$	1,116.03 $_{3f}$	1,457.35 $_{2t}$	1,503.67 $_{2f/1t}$	450
TE3	87.50 $_{1t}$	151.59 $_{1f}$	360.40 $_{2f/1t}$	507.72 $_{2t}$	610.08 $_{2f/2t}$	798.29 $_{3f/1t}$	750
TE4	86.17 $_{1t}$	143.74 $_{1f/2t}$	266.17 $_{2t}$	342.65 $_{2f/1t}$	403.59 $_{2f/2t}$	732.00 $_{3f}$	1125
TE5	84.84 $_{1t}$	137.83 $_{1f/2t}$	243.92 $_{2t}$	340.25 $_{2f/1t}$	384.88 $_{2f/2t}$	575.75 $_{3t}$	1575
TE6	84.72 $_{1t}$	137.31 $_{1f/2t}$	242.73 $_{2t}$	338.82 $_{2f/1t}$	380.34 $_{2f/2t}$	525.66 $_{3t}$	2100
LE9	84.67 $_{1t}$	137.16 $_{1f/2t}$	242.48 $_{2t}$	338.06 $_{2f/1t}$	379.07 $_{2f/2t}$	514.94 $_{3t}$	12375
Exp. [15]	85.6	134.5	259.0	351.0	395.0	514.94	-
Shell [15]	85.9	137.8	248.6	342.9	387.4	531.9	-
Shell FEM [32]	85.7	138.4	249.9	346.4	389.5	541.0	3456
FEM 3D [21]	84.8	137.3	240.9	338.4	377.8	507.1	6354

Table 2: Natural frequencies [Hz] of the rotating isotropic blade by using different theories. $_f$: flapwise, $_l$: chordwise, $_t$: torsional frequency.

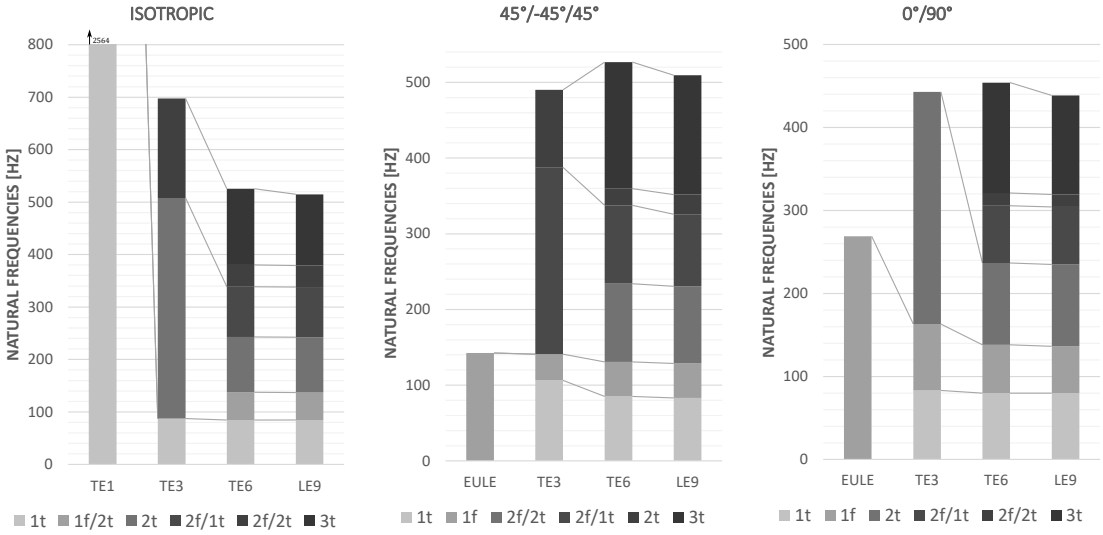

Figure 5: Comparisons of the frequencies between Taylor-type and Lagrange-type models for different stacking sequences

			0° / 90° / 0°				**DoFs**
EBBT	310.20 $_{1f}$	1,933.39 $_{2f}$	3,924.59 $_{1l}$	5,366.82 $_{3f}$	7,222.93	10,387.94 $_{4f}$	75
FSDT	305.72 $_{1f}$	1,628.78 $_{1l}$	1,761.94 $_{2f}$	4,425.80 $_{3f}$	4,794.14 $_{2l}$	7,222.93	125
TE1	308.76 $_{1f}$	1,631.52 $_{1l}$	1,777.09 $_{2f}$	1,735.04 $_{1t}$	4,459.92 $_{3f}$	4,811.47 $_{2l}$	225
TE2	208.70 $_{1f}$	395.62 $_{1t}$	687.27 $_{2f}$	1,319.80 $_{2t}$	1,340.96 $_{3f}$	1,630.92 $_{1l}$	450
TE3	102.90 $_{1t}$	178.47 $_{1f}$	443.69 $_{2t}$	454.19 $_{2f/1t}$	634.10 $_{2f}$	1,094.88 $_{3f/1t}$	750
TE4	100.56 $_{1t}$	141.71 $_{1f/2t}$	243.74 $_{2t}$	442.56 $_{2f/1t}$	452.50 $_{2f/2t}$	639.32 $_{3t}$	1125
TE5	99.60 $_{1t}$	129.35 $_{1f/2t}$	238.00 $_{2t}$	376.56 $_{3t}$	439.40 $_{2f/2t}$	441.61 $_{2f/1t}$	1575
TE6	99.09 $_{1t}$	128.56 $_{1f/2t}$	237.76 $_{2t}$	341.80 $_{3t}$	436.69 $_{2f/2t}$	436.35 $_{2f/1t}$	2100
LE9	98.94 $_{1t}$	127.52 $_{1f/2t}$	237.23 $_{2t}$	323.19 $_{3t}$	434.21 $_{2f/1t}$	435.26 $_{2f/2t}$	17325
			45° / −45° / 45°				
EBBT	142.45 $_{1f}$	888.18 $_{2f}$	1,834.06 $_{1l}$	2,466.78 $_{3f}$	3,305.63	4,778.20 $_{4f}$	75
FSDT	142.06 $_{1f}$	871.63 $_{2f}$	1,540.76 $_{1l}$	2,364.09 $_{3f}$	3,229.04	4,438.57 $_{4f}$	125
TE1	206.64 $_{1f}$	1,250.94 $_{2f}$	1,830.38 $_{1l}$	2,330.30 $_{2l}$	3,285.81 $_{1t}$	3,753.05 $_{3f}$	225
TE2	162.23 $_{1f}$	496.39 $_{1t}$	637.13 $_{2f}$	1,028.03 $_{3f}$	1,216.68 $_{2t}$	1,432.28 $_{4f}$	450
TE3	106.34 $_{1t}$	140.93 $_{1f}$	387.73 $_{2f/1t}$	490.26 $_{2t}$	631.23 $_{2f/2t}$	810.72 $_{3f/1t}$	750
TE4	89.15 $_{1t}$	133.81 $_{1f}$	251.13 $_{2f/2t}$	371.49 $_{2f/1t}$	428.96 $_{2t}$	718.77 $_{3f}$	1125
TE5	85.42 $_{1t}$	131.16 $_{1f}$	234.70 $_{2f/2t}$	343.55 $_{2f/1t}$	369.28 $_{2t}$	557.69 $_{3t}$	1575
TE6	85.21 $_{1t}$	130.86 $_{1f}$	233.98 $_{2t/2t}$	337.43 $_{2f/1t}$	359.74 $_{2t}$	526.76 $_{3t}$	2100
LE9	83.21 $_{1t}$	128.65 $_{1f}$	230.79 $_{2f/2t}$	325.63 $_{2f/1t}$	351.60 $_{2t}$	509.52 $_{3t}$	17325
			45° / 0° / −45°				
EBBT	241.24 $_{1f}$	1,503.98 $_{2f}$	3,105.11 $_{1l}$	4,176.40 $_{3f}$	5,617.17	8,087.93 $_{4f}$	75
FSDT	239.05 $_{1f}$	1,423.91 $_{2f}$	1,943.81 $_{1l}$	3,713.03 $_{3f}$	5,315.15 $_{2l}$	5,620.02	125
TE1	270.22 $_{1f}$	1,602.34 $_{2f}$	1,834.70 $_{1t}$	2,738.07 $_{1l/1t}$	4,113.86 $_{3f}$	5,526.36 $_{1l}$	225
TE2	226.19 $_{1f}$	504.19 $_{1t}$	732.60 $_{2f}$	1,057.12 $_{3f}$	1,208.81 $_{2t}$	1,319.50 $_{4f}$	450
TE3	99.11 $_{1t}$	197.13 $_{1f}$	403.50 $_{2f/1t}$	473.06 $_{2t}$	664.17 $_{1f/2t}$	795.95 $_{3f/1t}$	750
TE4	97.13 $_{1t}$	152.08 $_{1f}$	272.03 $_{2t}$	399.52 $_{1f/2t}$	388.16 $_{2f/1t}$	717.98 $_{2f/3t}$	1125
TE5	95.77 $_{1t}$	139.67 $_{1f}$	259.87 $_{2t}$	372.25 $_{2f/1t}$	380.44 $_{2f/2t}$	451.44 $_{3t}$	1575
TE6	95.42 $_{1t}$	137.74 $_{1f/2t}$	258.60 $_{2t}$	374.53 $_{2f/2t}$	361.59 $_{2f/1t}$	419.40 $_{3t}$	2100
LE9	102.60 $_{1t}$	148.48 $_{1f/2t}$	278.06 $_{2t}$	368.51	439.13 $_{2f/2t}$	503.98 $_{3t}$	17325

Table 3: Natural frequencies [Hz] for triple-layers composite blade by different theories
$_f$: flapwise, $_l$: chordwise, $_t$: torsional frequency.

			0° / 0°				**DoFs**
EBBT	372.69 $_{1f}$	2,322.94 $_{2f}$	4,737.30 $_{1l}$	6,448.30 $_{3f}$	8,718.03	12,481.63 $_{4f}$	75
FSDT	364.98 $_{1f}$	1,661.06 $_{1l}$	2,040.96 $_{2f}$	4,938.68 $_{2l}$	4,979.15 $_{3f}$	8,400.22 $_{4f}$	125
TE1	367.33 $_{1f}$	1,662.27 $_{1l}$	2,051.85 $_{2f}$	1,735.04 $_{1t}$	4,949.27 $_{2l}$	5,004.09 $_{3f}$	225
TE2	214.76 $_{1f}$	422.79 $_{1t}$	600.27 $_{2f}$	858.49 $_{2t}$	1,152.52 $_{3f}$	1,661.71 $_{1l}$	450
TE3	109.10 $_{1t}$	180.25 $_{1f/2t}$	447.46 $_{2t}$	455.28 $_{2f/1t}$	550.17 $_{2f/2t}$	1,081.72 $_{3f/1t}$	750
TE4	105.18 $_{1t}$	133.87 $_{1f/2t}$	239.15 $_{2t}$	441.75 $_{2f/1t}$	451.20 $_{2f/2t}$	629.78	1125
TE5	104.33 $_{1t}$	122.28 $_{1f/2t}$	235.69 $_{2t}$	329.15 $_{3t}$	440.03 $_{2f/2t}$	440.29 $_{2f/1t}$	1575
TE6	103.90 $_{1t}$	121.20 $_{1f/2t}$	235.47 $_{2t}$	290.90 $_{3t}$	436.98 $_{2f/2t}$	435.75 $_{2f/1t}$	2100
LE9	103.73 $_{1t}$	120.86 $_{1f/2t}$	235.36 $_{2t}$	282.95 $_{3t}$	436.11 $_{2f/2t}$	434.50 $_{2f/1t}$	12375
			0° / 90°				
EBBT	268.87 $_{1f}$	1,676.03 $_{2f}$	3,454.78$_{1l}$	4,653.33 $_{3f}$	6,338.34	9,009.96 $_{4f}$	75
FSDT	265.93 $_{1f}$	1,560.56 $_{2f}$	1,598.68$_{1l}$	3,997.82 $_{3f}$	4,647.34 $_{2l}$	6,337.28	125
TE1	268.35 $_{1f}$	1,573.24 $_{2f}$	1,601.12$_{1l}$	1,735.04 $_{1t}$	4,027.57 $_{3f}$	4,663.04 $_{2l}$	225
TE2	188.22 $_{1f}$	369.39 $_{1t}$	602.81$_{2f}$	1,072.71 $_{3f}$	1,448.15 $_{2t}$	1,524.09 $_{4f}$	450
TE3	83.11 $_{1t}$	163.09 $_{1f}$	323.85$_{2f/1t}$	442.86 $_{2t}$	544.99 $_{2f}$	688.22 $_{3f/1t}$	750
TE4	81.40 $_{1t}$	147.96 $_{1f}$	248.34$_{2t}$	311.72 $_{2f/1t}$	345.16 $_{2f/2t}$	659.12 $_{3f/2t}$	1125
TE5	80.00 $_{1t}$	138.50 $_{1f}$	236.90$_{2t}$	309.87 $_{2f/1t}$	324.58 $_{2f/2t}$	466.25 $_{3t}$	1575
TE6	79.82 $_{1t}$	138.00 $_{1f}$	236.61$_{2t}$	305.76 $_{2f/1t}$	321.07 $_{2f/2t}$	454.12 $_{3t}$	2100
LE9	79.74 $_{1t}$	136.30 $_{1f}$	234.92$_{2t}$	304.23 $_{2f/1t}$	319.06 $_{2f/2t}$	438.69 $_{3t}$	12375
			90° / 90°				
EBBT	90.45 $_{1f}$	563.96 $_{2f}$	1,162.05 $_{1l}$	1,566.43 $_{3f}$	2,104.15	3,034.46 $_{4f}$	75
FSDT	90.33 $_{1f}$	559.15 $_{2f}$	1,006.80 $_{1l}$	1,535.85 $_{3f}$	2,104.15	2,931.07 $_{4f}$	125
TE1	94.47 $_{1f}$	584.38 $_{2f}$	1,037.29 $_{1l}$	1,603.66 $_{3f}$	1,735.04 $_{1t}$	2,113.94	225
TE2	85.47 $_{1f}$	273.18 $_{1t}$	406.12 $_{2f}$	834.69 $_{3f}$	907.80 $_{2f/1t}$	996.70 $_{1l}$	450
TE3	52.21 $_{1t}$	82.66 $_{1f}$	203.99 $_{2f/1t}$	363.28 $_{2f}$	452.14 $_{3f/1t}$	505.69 $_{2t}$	750
TE4	51.79 $_{1t}$	82.23 $_{1f}$	199.82 $_{2f/1t}$	313.65 $_{2f}$	358.01 $_{2t}$	434.72 $_{3f/1t}$	1125
TE5	51.12 $_{1t}$	82.14 $_{1f}$	197.46 $_{2f/1t}$	306.85 $_{2f}$	347.76 $_{2t}$	432.46 $_{3f/1t}$	1575
TE6	51.09 $_{1t}$	82.12 $_{1f}$	197.28 $_{2f/1t}$	305.47 $_{2f}$	345.61 $_{2t}$	430.56 $_{3f/1t}$	2100
LE9	51.07 $_{1t}$	82.11 $_{1f}$	197.21 $_{2f/1t}$	305.39 $_{2f}$	345.57 $_{2t}$	430.21 $_{3f/1t}$	12375
			45° / −45°				
EBBT	142.45 $_{1f}$	888.19 $_{2f}$	1,834.54 $_{1l}$	2,466.90 $_{3f}$	3,305.90	4,778.64 $_{4f}$	75
FSDT	141.66 $_{1f}$	869.37 $_{2f}$	1,557.10 $_{1l}$	2,358.41 $_{3f}$	3,305.89	4,429.39 $_{4f}$	125
TE1	207.41 $_{1f}$	1,258.94 $_{2f}$	1,831.00 $_{1l}$	2,370.16 $_{1t}$	3,308.85 $_{3f}$	3,785.62	225
TE2	163.33 $_{1f}$	503.44 $_{1t}$	630.80 $_{2f}$	966.99 $_{3f}$	1,203.49 $_{4f/2t}$	1,241.69 $_{4f}$	450
TE3	85.59 $_{1t}$	138.92 $_{1f}$	345.23 $_{2f/1t}$	444.53 $_{2t}$	615.36 $_{2f}$	740.28 $_{3f/1t}$	750
TE4	83.44 $_{1t}$	125.29 $_{1f}$	223.66 $_{2t}$	337.67 $_{2f/1t}$	378.86 $_{2f/2t}$	673.16 $_{3f}$	1125
TE5	82.19 $_{1t}$	119.68 $_{1f}$	209.65 $_{2t}$	326.59 $_{2f/1t}$	359.41 $_{2f/2t}$	459.82 $_{3t}$	1575
TE6	81.50 $_{1t}$	118.31 $_{1f}$	207.53 $_{2t}$	320.61 $_{2f/1t}$	349.64 $_{2f/2t}$	420.98 $_{3t}$	2100
LE9	79.69 $_{1t}$	116.90 $_{1f}$	205.06 $_{2t}$	312.30 $_{2f/1t}$	341.28 $_{2f/2t}$	407.53 $_{3t}$	12,325

Table 4: Natural frequencies [Hz] for double-layers composite blade by different theories
$_f$: flapwise, $_l$: chordwise, $_t$: torsional frequency.

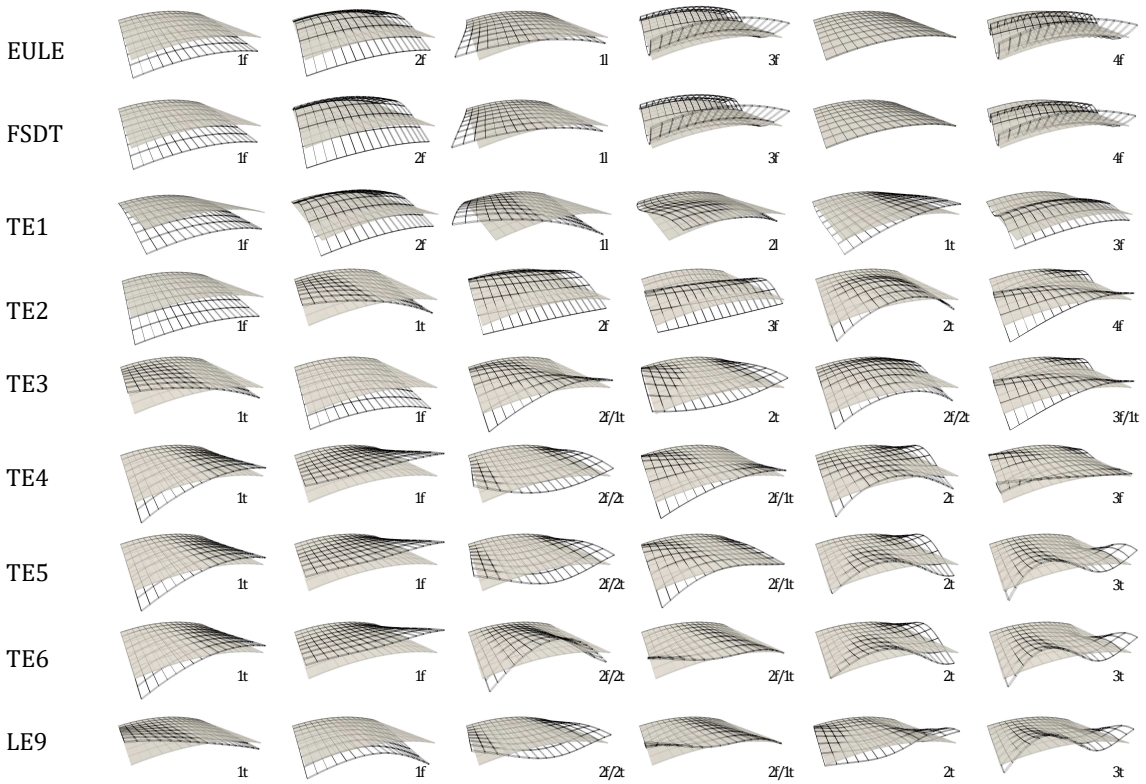

Figure 6: Mode shapes for the $[45°/-45°/45°]$ composite blade

The number of degrees-of-freedom (DoFs) for each structural model is also given in Tab. 2, 4 and 3, in order to show the numerical efficiency of the approaches. For bending modes, with a slight torsional deformation, EBBT and FSDT models provided acceptable results with high computational saving. It is interesting to note that a mode shape mainly dominated by bending deformation appears only in some types of lamination schemes. The third-order Taylor theory TE3 provided comparable results with more refined theories for the 1^{st} (torsional mode) and 2^{nd} (bending mode usually coupled with a torsional one) frequencies. Also in this case, the computational saving was considerable; DoFs were reduced by 2.8 and 23.1 times compared to TE6 and LE9 models, respectively. The forth-order Taylor theory TE4 predicted frequencies with high precision up to the second torsional frequency; for following modes TE4 overestimated the frequencies values. Moreover, it is worth note that frequencies predicted by the TE5 e TE6 theory are essentially the same compared to those calculated with LE9 models. Comparing the degrees of freedom,

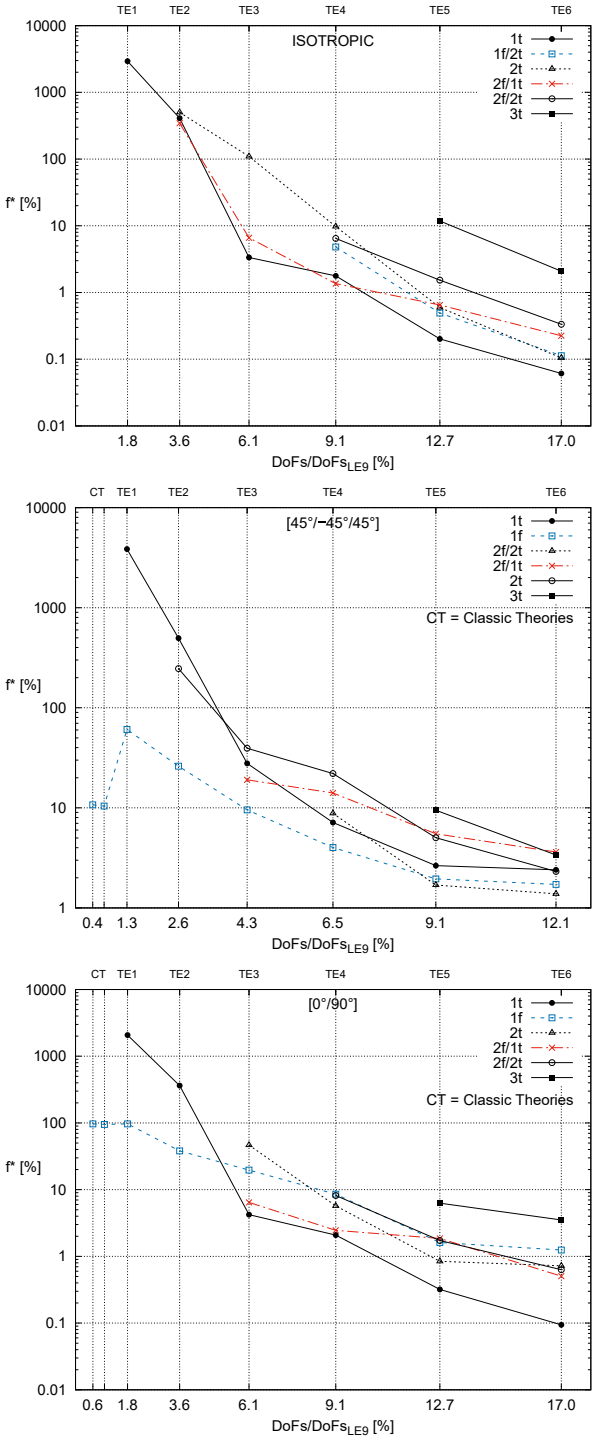

Figure 7: Errors on natural frequencies versus DoFs savings with $f^* = (f - f_{LE9})/f_{LE9}$ - Logarithmic scale on y axis

it is evident that the TE models are computationally advantageous with respect to the LW solutions.

In Fig. 7 the effects of the order of approximation are shown in terms of percentage error. The trend is related to the computational savings of each theory compared to the LE9 theory. Through these plots, it is possible to evaluate the effectiveness of a given kinematic model in terms of accuracy and computational cost with respect to a reference solution.

The correspondence of mode shapes related to different orientation angles has been investigated by using the Modal Assurance Criterion (MAC), whose graphic representation is shown in Fig. 10. MAC matrix shows a low similarity between the various mode shapes for the different configurations; in most cases, the MAC value is very different from the unit. As expected, the MAC matrices show sparse correlations due to coupling phenomena for the various stacking sequences. Eigenvectors have little correspondence with the others, thus demonstrating that the fibers lamination angle has an important effect on the deformation modes.

It is interesting to study the effect of thickness on the rotating blade. In Tab. 5 the natural frequencies are listed for three significant stacking sequences for $t = L/50$. The most evident effect is a general increase of the frequencies that settles around 60% compared to the thinner case. The mode shapes detected are essentially the same, for some modes there is an exchange in the order of appearance. In Fig. 8 the effects of the computational cost of each model versus the errors on the solutions are shown. Of course, for higher modes, the difference would become greater. One note that significant differences are found only in [45° / −45° / 45°] stacking sequence case. A clear representation is provided in Fig. 9. For thin blade the first bending frequency is well computed both with EBBT and FSDT theories, instead for thick blade the FSDT theory provide worse results. The *1f/2t* trend is almost the same for both blade thicknesses, but the cubic expansion for the thick case seems to provide highly accurate values even better than sixth order Taylor expansion. This result

			ISOTROPIC				**DoFs**
EBBT	204.84_{1f}	$1{,}275.06_{2f}$	$2{,}362.41_{1l}$	$3{,}532.15_{3f}$	4,134.70	$6{,}817.11_{4f}$	75
FSDT	236.72_{1f}	$1{,}440.26_{2f}$	$1{,}974.99_{1l}$	$3{,}857.43_{3f}$	4,797.24	$5{,}127.09_{2l}$	125
TE1	236.72_{1f}	$1{,}440.56_{2f}$	$1{,}975.72_{1l}$	$2{,}564.23_{1t}$	$3{,}863.16_{3f}$	4,189.16	225
TE2	192.11_{1f}	477.53_{1t}	760.14_{2f}	$1{,}459.31_{3f}$	$1{,}612.40_{2t}$	$1{,}686.64_{2f/1t}$	450
TE3	146.08_{1t}	178.77_{1f}	$574.88_{2f/1t}$	656.27_{2f}	784.68_{2t}	$1{,}334.08_{3f}$	750
TE4	143.50_{1t}	$177.67_{1f/2t}$	440.51_{2t}	$551.85_{2f/1t}$	644.93_{2f}	$1{,}004.75_{2f/2t}$	1,125
TE5	141.29_{1t}	$175.57_{1f/2t}$	398.16_{2t}	$545.28_{2f/1t}$	630.29_{2f}	$985.17_{2f/2t}$	1,575
TE6	141.02_{1t}	$175.36_{1f/2t}$	394.90_{2t}	$544.19_{2f/1t}$	623.58_{2f}	931.44_{3t}	2,100
LE9	140.76_{1t}	$175.15_{1f/2t}$	392.40_{2t}	$543.14_{2f/1t}$	620.45_{2f}	903.95_{3t}	12375
			0° / 90°				
EBBT	306.85_{1f}	$1{,}908.95_{2f}$	$3{,}597.29_{1l}$	$5{,}283.05_{3f}$	6,336.25	$10{,}186.51_{4f}$	75
FSDT	305.40_{1f}	$1{,}613.57_{1l}$	$1{,}756.70_{2f}$	$4{,}394.66_{3f}$	$4{,}677.81_{2l}$	6,391.16	125
TE1	305.34_{1f}	$1{,}614.49_{1l}$	$1{,}757.56_{2f}$	$1{,}735.04_{1t}$	$4{,}412.69_{3f}$	$4{,}697.50_{2l}$	225
TE2	213.71_{1f}	409.57_{1t}	720.72_{2f}	$1{,}388.62_{3f}$	$1{,}537.57_{2t}$	$1{,}613.46_{2l}$	450
TE3	122.29_{1t}	192.67_{1f}	$489.72_{2f/1t}$	625.66_{2t}	666.40_{2f}	$1{,}115.84_{3f/1t}$	750
TE4	121.51_{1t}	191.39_{1f}	387.00_{2t}	$480.17_{2f/1t}$	$579.33_{2f/2t}$	$845.82_{3f/2t}$	1,125
TE5	118.59_{1t}	187.47_{1f}	354.82_{2t}	$474.48_{2f/1t}$	$559.20_{2f/2t}$	834.31_{3t}	1,575
TE6	118.42_{1t}	186.94_{1f}	353.19_{2t}	$472.66_{2f/1t}$	$547.55_{2f/2t}$	808.46_{3t}	2,100
LE9	118.23_{1t}	185.82_{1f}	346.80_{2t}	$471.37_{2f/1t}$	$542.18_{2f/2t}$	770.11_{3t}	12375
			45° / −45° / 45°				
EBBT	138.72_{1f}	865.16_{2f}	$1{,}791.04_{1l}$	$2{,}403.82_{3f}$	3,305.63	$4{,}658.83_{4f}$	75
FSDT	204.86_{1f}	$1{,}244.48_{2f}$	$2{,}277.30_{1l}$	$3{,}327.61_{3f}$	4,724.06	$6{,}124.91_{4f}$	125
TE1	202.15_{1f}	$1{,}225.36_{2f}$	$1{,}819.34_{1t}$	$2{,}296.41_{1l/1t}$	$3{,}228.73_{3f}$	$3{,}740.06_{4f}$	225
TE2	161.49_{1f}	503.37_{1t}	707.47_{2f}	$1{,}318.89_{3f}$	$1{,}368.59_{2t}$	$1{,}615.60_{4f}$	450
TE3	138.35_{1f}	195.58_{1t}	$589.02_{2f/1t}$	633.49_{2t}	$860.82_{2f/2t}$	$1{,}205.23_{3f}$	750
TE4	133.83_{1f}	171.85_{1t}	$435.12_{2f/2t}$	$556.70_{2f/1t}$	695.33_{2t}	$1{,}017.86_{3f}$	1,125
TE5	131.66_{1f}	169.63_{1t}	$404.01_{2f/2t}$	$537.86_{2f/1t}$	657.39_{2t}	963.95_{3t}	1,575
TE6	130.88_{1f}	169.09_{1t}	$401.02_{2f/2t}$	$531.98_{2f/1t}$	639.61_{2t}	923.47_{3t}	2,100
LE9	127.56_{1f}	165.41_{1t}	$391.83_{2f/2t}$	$513.97_{2f/1t}$	621.57_{2t}	889.13_{3t}	17325

Table 5: Natural frequencies [Hz] for triple-layers composite blade by different theories - Thickness equal to $L/50$. $_f$: flapwise, $_l$: chordwise, $_t$: torsional frequency.

may have been altered by comparison of non-identical modal shapes.

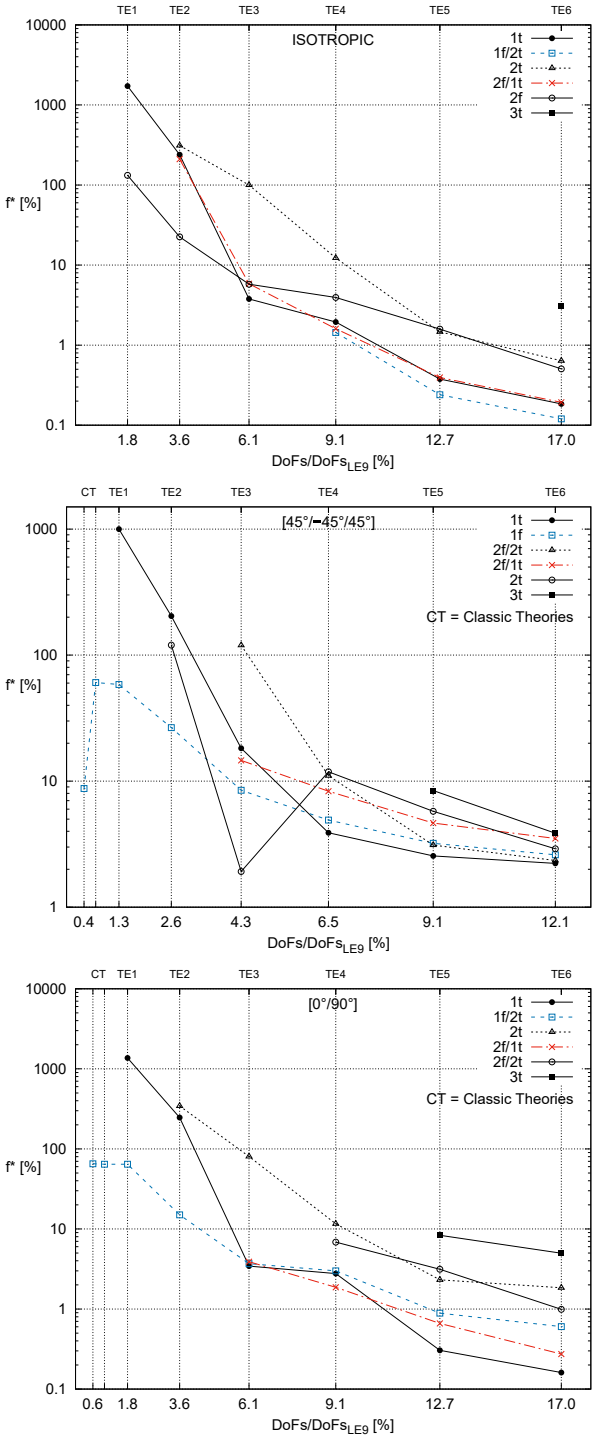

Figure 8: Error on natural frequencies versus DoFs savings for thick blade ($t = L/50$) with $f^* = (f - f_{LE9})/f_{LE9}$ - Logarithmic scale on y axis

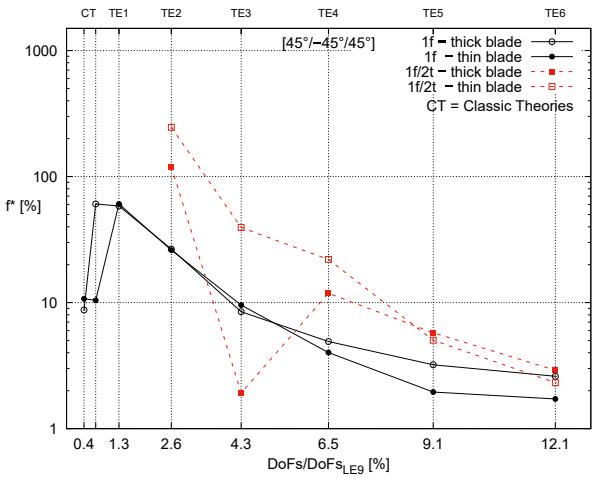

Figure 9: Error comparison between thick blade ($t = L/50$) and thin blade ($t = L/100$) with $f^* = (f - f_{LE9})/f_{LE9}$ - Logarithmic scale on y axis

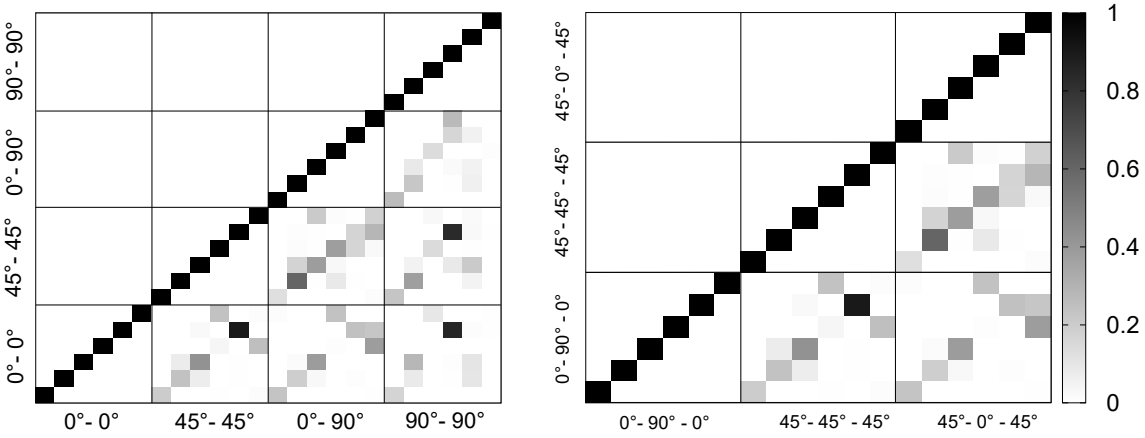

Figure 10: MAC between different lamination schemes - LE9 models

3.4. Rotating blades

Figure 11 shows the frequency values computed with TE4, TE5, TE6 and LE9 models as function of the rotational speed for the $[45°/-45°/45°]$ configuration. To enable the comparison with the results presented in Ref. [21, 32], the circular frequencies (ω) and the speed have been reported in the following nondimensional forms $\omega_n^* = \omega_n(\sqrt{12\rho L^4(1-\nu^2)/Et^2})$ and $\Omega^* = \Omega/\omega_1$, where ω_1 is the natural frequency, E the Young module for an isotropic plate and ν the Poisson coefficient. These Campbell diagrams demonstrate the differences between the various computational models. Indeed, for the TE4 model, the first frequencies trend revealed a considerable agreement with LE9; instead, some discrepancies can be observed for higher frequencies. Rising the Taylor expansions order can be highlighted as an increasing similarity between the models.

It is interesting to note that, varying the fibers' lamination angle, mode shapes are different with the increasing rotational speed. Fig 12 and 13 show a MAC comparison between two different nondimensional rotational speed, for $[45°/-45°/45°]$ and $[0°/90°/0°]$ configurations respectively. In the latter case a mode exchange among the first two frequencies can be pointed out. Therefore the lamination angle influences the shape of the vibration modes as the rotation speed changes.

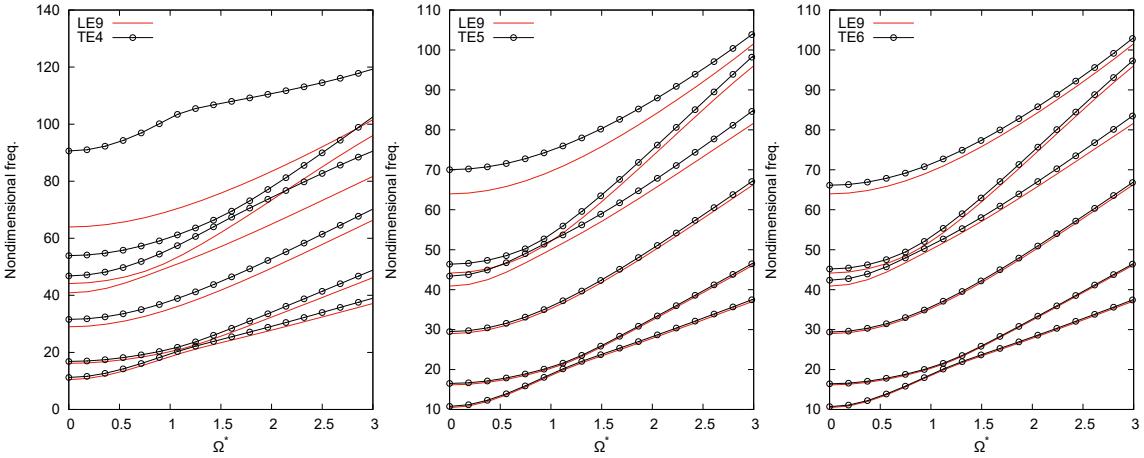

Figure 11: Evolution of natural frequencies versus rotational speed for the $[45°/-45°/45°]$ composite blade

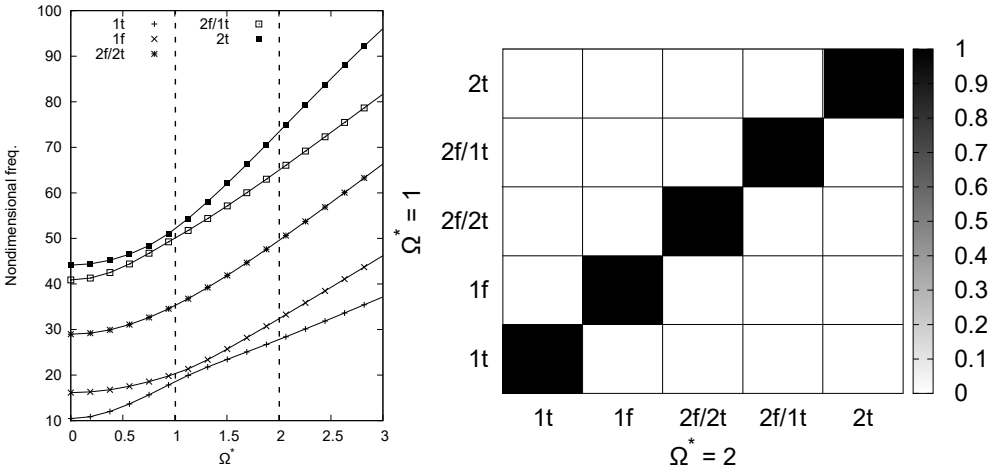

Figure 12: MAC between different values of Ω^* for the $[45°/-45°/45°]$ composite blade by LE9 model

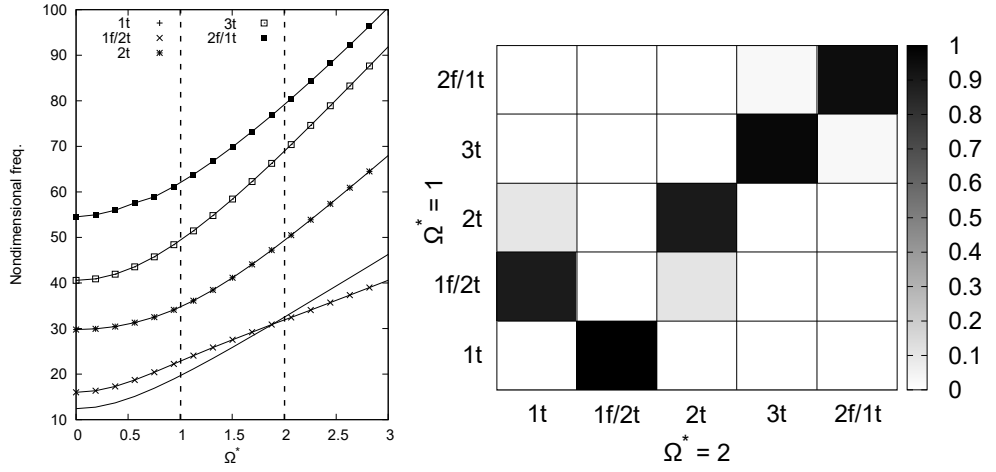

Figure 13: MAC between different values of Ω^* for the $[0°/90°/0°]$ composite blade by LE9 model

4. Conclusions

In the present paper, refined theories have been used to study the dynamic response of composite rotating blades. Several structural models and lamination schemes have been considered to assess their accuracy. In light of the proposed results, it is possible to draw the following conclusions:

1. For both the isotropic and orthotropic blades, the use of finite elements based on higher beam models leads to accurate results regardless of the lamination scheme.
2. Classical theories yield acceptable qualitative results for a limited range of problems.
3. Higher-than-sixth-order TE models provide natural frequencies values similar to the LE9 reference model, with a high computational saving.
4. When torsional or bending-torsional coupling mode shapes occur, higher theories are mandatory to predict correct values of frequencies.
5. For TE higher-order models, frequencies as a function of the rotational speed show an analog trend with the LE9 models.
6. The lamination scheme affects the dynamic behavior of the blade. For rotating structures, different lamination cause a frequency switching that does not appear for every stacking sequences.
7. An increase in thickness leads to frequencies at higher values. Among the different structures with several thickness the modes of vibrating are very similar in most cases.

The results obtained can be used as a benchmark for future studies, furthermore this study lays the basis for further analysis, such as the study of the time response of a rotating plate.

References

[1] J.S. Rao.

Natural frequencies of turbine blading-a survey.

Shock and Vibration Digest, 5(10):3–16, 1973.

[2] S. Putter and H. Manor.

Natural frequencies of radial rotating beams.

Journal of Sound and Vibration, 56(2):175–185, 1978.

[3] R. Chandra and I. Chopra.

Experimental-theoretical investigation of the vibration characteristics of rotating composite box beams.

Journal of Aircraft, 29(4):657–664, 1992.

[4] C. Cesnik and D.H. Hodges.

Vabs: a new concept for composite rotor blade cross-sectional modeling.

Journal of the American helicopter society, 42(1):27–38, 1997.

[5] D.H. Hodges.

Nonlinear composite beam theory.

Progress in astronautics an aeronautics, 2006.

[6] Y.J Kee and J. Kim.

Vibration characteristics of initially twisted rotating shell type composite blades.

Composite structures, 64(2):151–159, 2004.

[7] X.X. Hu, T. Sakiyama, H. Matsuda, and C. Morita.

Fundamental vibration of rotating cantilever blades with pre-twist.

Journal of sound and vibration, 271(1-2):47–66, 2004.

[8] H. Kang, C. Chang, H. Saberi, and R.A. Ormiston.
Assessment of beam and shell elements for modeling rotorcraft blades.
Journal of Aircraft, 51(2):520–531, 2014.

[9] W. Yu, D. H. Hodges, and V. V. Volovoi.
Asymptotic generalization of reissner–mindlin theory: accurate three-dimensional recovery for composite shells.
Computer Methods in Applied Mechanics and Engineering, 191(44):5087–5109, 2002.

[10] O.A. Bauchau, C.L. Bottasso, and Y.G. Nikishkov.
Modeling rotorcraft dynamics with finite element multibody procedures.
Mathematical and Computer Modelling, 33(10-11):1113–1137, 2001.

[11] O.A. Bauchau and W. Chiang.
Dynamic analysis of bearingless tail rotor blades based on nonlinear shell models.
Journal of Aircraft, 31(6):1402–1410, 1994.

[12] O.A. Bauchau, J.Y. Choi, and C.L. Bottasso.
On the modeling of shells in multibody dynamics.
Multibody System Dynamics, 8(4):459–489, 2002.

[13] A.W. Leissa and M.S. Ewing.
Comparison of beam and shell theories for the vibrations of thin turbomachinery blades.
ASME 1982 International Gas Turbine Conference and Exhibit, 1983.

[14] A.W. Leissa.

Vibrational aspects of rotating turbomachinery blades.
Applied Mechanics Reviews, 34(5):629–635, 1981.

[15] A. W. Leissa, J. K. Lee, A.J. Wang.
Rotating blade vibration analysis using shells
Journal of Engineering for Power, 104(2):296–302, 1982.

[16] M. S. Qatu and A. W. Leissa.
Vibration studies for laminated composite twisted cantilever plates.
International Journal of Mechanical Sciences, 33(11):927–940,
1991.

[17] J. Sun, I. L. Arteaga, and L. Kari.
Dynamic modeling of a multilayer rotating blade via quadratic
layerwise theory.
Composite Structures, 99():276–287, 2013.

[18] E. Carrera, M. Filippi, and E. Zappino.
Free vibration analysis of rotating composite blades via carrera
unified formulation.
Composite Structures, 106():317–325, 2013.

[19] M. Filippi and E. Carrera.
Capabilities of 1D CUF-based models to analyse metallic/composite
rotors.
Advances in aircraft and spacecraft science, 3(1):1–14, 2016.

[20] E. Carrera, M. Filippi.
Variable kinematic one-dimensional finite elements for the analysis of rotors made of composite materials
Journal of Engineering for Gas Turbines and Power, 136(9):092–501, 2014.

[21] M. Filippi, A. Pagani, E. Carrera.

Accurate nonlinear dynamics and mode aberration of rotating blades
Journal of Applied Mechanics, 85(11):111004, 2018.

[22] E. Carrera, M. Cinefra, M. Petrolo, E. Zappino.
Finite element analysis of structures through unified formulation
John Wiley & Sons, 2014.

[23] E. Carrera.
Historical review of zig-zag theories for multilayered plates and shells
Appl. Mech. Rev., 56(3):287–308, 2003.

[24] I. Kreja.
A literature review on computational models for laminated composite and sandwich panels
Open Engineering, 1(1):59–80, 2011.

[25] J.N. Reddy.
Mechanics of laminated composite plates and shells: theory and analysis
CRC press, 2003.

[26] E. Carrera, G. Giunta, M. Petrolo.
Beam structures: classical and advanced theories
John Wiley & Sons, 2011.

[27] E. Carrera.
Theories and finite elements for multilayered, anisotropic, composite plates and shells
Archives of Computational Methods in Engineering, 9(2):87–140, 2002.

[28] E. Carrera.
Theories and finite elements for multilayered, anisotropic, composite plates and shells
Archives of Computational Methods in Engineering, 9(2):87–140, 2002.

[29] E. Carrera, M. Petrolo.

Refined beam elements with only displacement variables and plate/shell capabilities

Meccanica, 47(3):537–556, 2012.

[30] E. Carrera, M. Filippi, E. Zappino.

Analysis of rotor dynamic by one-dimensional variable kinematic theories

Journal of engineering for gas turbines and power, 135(9):, 2012.

[31] E. Carrera, M. Filippi.

A refined one-dimensional rotordynamics model with three-dimensional capabilities

Journal of Sound and Vibration, 366():343–356, 2016.

[32] Y.J. Kee, S.J. Shin.

Structural dynamic modeling for rotating blades using three dimensional finite elements

Journal of Mechanical Science and Technology, 29(4):1607–1618, 2015.